I-AUV Docking and Intervention in a Subsea Panel

Narcís Palomeras[1], Antonio Peñalver[2], Miquel Massot-Campos[3], Guillem Vallicrosa[1], Pep Lluís Negre[3], J. Javier Fernández[2], Pere Ridao[1], Pedro J. Sanz[2], Gabriel Oliver-Codina[3], Albert Palomer[1].

***Abstract*— While commercially available autonomous underwater vehicles (AUVs) are routinely used in survey missions, a new set of applications exist which clearly demand intervention capabilities: the maintenance of permanent underwater structures as well as the recovery of benthic stations or black-boxes are a few of them. These tasks are addressed nowadays using manned submersibles or work-class remotely operated vehicles (ROVs), equipped with teleoperated arms under human supervision. In the context of the TRITON Spanish funded project, a subsea panel docking and an intervention procedure are proposed. The light-weight intervention AUV (I-AUV) Girona 500 is used to autonomously dock into a subsea panel using a funnel-based docking method for passive accommodation. Once docked, an autonomous fixed-based manipulation system, which uses feedback from a digital camera, is used to turn a valve and plug/unplug a connector. The paper presents the techniques used for the autonomous docking and manipulation as well as how the adapted subsea panel has been designed to facilitate such operations.**

I. INTRODUCTION

A large number of applications exist in the underwater domain that go beyond the survey capabilities. The maintenance of permanent observatories, submerged oil wells, cabled sensor networks, pipes, and the deployment and recovery of benthic stations, or the search and recovery of black-boxes are just some of them. Nowadays, these tasks require the use of work-class remotely operated vehicles (ROVs) deployed from dynamic positioning (DP) vessels making them very expensive. Despite several underwater intervention systems were developed during the 90's [1], [2], [3], [4], it was not until the 1st decade of the 21th century that field demonstrations arrived.

Very successful approaches were based on hybrid ROV/AUV concepts like the one proposed by the SWIMMER project [5] where an AUV shuttle transporting a ROV, autonomously homes and docks into a seabed docking station. Next, the ROV, which is connected through the docking device to a remote operation station, is teleoperated during the intervention. The system avoids the need for a DP capable ship with the consequent savings.

Recently, another hybrid concept appeared, the hybrid ROVs (HROVs) [6], [7]. These vehicles are essentially AUVs reconfigurable as ROVs when tethered through an optical fiber umbilical. Thanks to its ultra light umbilical, HROVs may also be operated from ships of opportunity without DP. When plugged, HROVs behave as conventional ROVs avoiding some of the difficulties related to the cable. Moreover, they have the capability of detaching the cable and surfacing autonomously.

Nevertheless, both systems keep the human within the control loop. The first fully autonomous intervention at sea, was demonstrated by the ALIVE project [8], where a hovering capable AUV was able to home to a subsea intervention panel using an imaging sonar, and then, docking into it with hydraulic grasps using visual feedback. Once attached to the panel, a very simple manipulation strategy (fixed base manipulation) was used to open/close a valve. First object manipulation from a floating vehicle (an I-AUV) was achieved in 2009 within SAUVIM project [9]. It was demonstrated the capability of searching for an object whose position was roughly known *a priori*. The object was endowed with artificial landmarks and the robot autonomously located it and hooked it with a recovery device while hovering. Finally, the first multipurpose object search and recovery strategy was demonstrated in the TRIDENT project in 2012. First, the object was searched using a down-looking camera and photo-mosaicing techniques. Next, it was demonstrated how to autonomously "hook" the object in a water tank [10]. The experiment was repeated in a harbor environment using a 4 degrees of freedom (DoF) arm [11], and later with a 7 DoF arm endowed with a 3 fingered hand [12] (see Fig. 1.(a)).

The TRITON project aims to demonstrate intervention capabilities in a permanent submerged observatory. The intervention tasks to demonstrate are: docking to an adapted subsea panel, fixed-based manipulation for valve turning and connector plugging/unplugging, and free floating manipulation for camera dome de-fouling (see Fig. 1.(b)). In this paper the first two tasks are presented.

Thus, given a subsea panel equipped with a docking mechanism, and a visual feature-rich panel to allow for real-time vision-based localization, the I-AUV has to start at a random position with the panel in the field of view (it is assumed to have reached the panel vicinity by acoustic means) and dock autonomously to the panel. Next, the I-AUV has to be able to complete an autonomous valve turning

*This work was supported by the Spanish project DPI2011-27977-C03v (TRITON).

[1]Universitat de Girona, Computer Vision and Robotics Institute, Centre d'Investigació en Robótica Submarina (CIRS), 17071 Girona (Spain) npalomer | gvallicrosa | pere@eia.udg.edu

[2]Universitat Jaume I, Interactive and Robotic Systems Laboratory (IRSLab), 12071 Castelló (Spain) penalvea | fernandj | sanzp@uji.es

[3]Universitat de les Illes Balears, Systems Robotics and Vision Group, 07122 Palma de Mallorca (Spain) pl.negre | miquel.massot | goliver@uib.cat

The University of Girona wants to thank the SARTI group for their collaboration in the TRITON project.

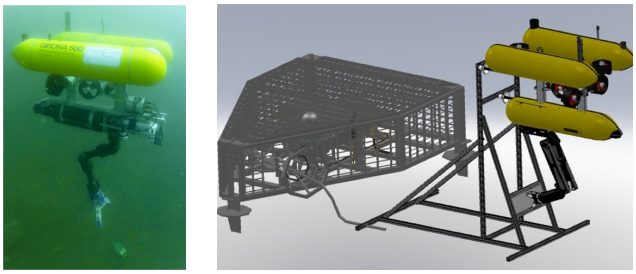

(a) (b)

Fig. 1: (a) TRIDENT project: Girona 500 I-AUV recovering a black-box with a 7 DoF manipulator autonomously. (b) TRITON concept: Girona 500 I-AUV docked in the subsea permanent observatory OBSEA.

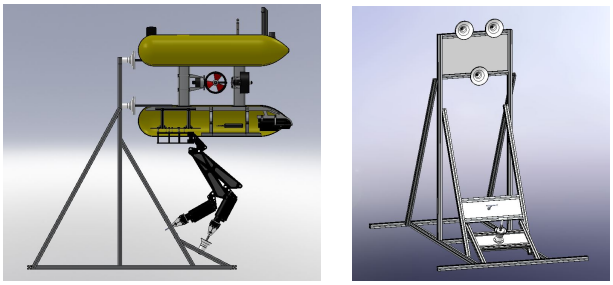

(a) (b)

Fig. 2: Schema of the mock-up intervention panel with (a) and without (b) the Girona 500 I-AUV docked.

and hot stab connector plugging/unplugging actions.

The paper is organized as follows. First, a funnel-based docking station developed for this project is presented. Next, the docking maneuver is split into: the panel detection by means of a vision-based algorithm and the docking maneuver. Section V details how the valve and the hot stab connector position are estimated while the manipulator initialization and the end-effector pose estimation are described in Section VI. Section VII introduces the procedures to turn a valve as well as to plug/unplug the hot stab connector. Once all the elements are presented, the results obtained in a water tank with the Girona 500 I-AUV are discussed in Section VIII before the conclusions.

II. I-AUV Friendly Docking Station

To design the mock-up AUV-friendly intervention panel, deliverables of the FREESUBNET network were used [13], [14]. The solution adopted for these deliverables was the installation of funnel-shaped receptacles in the panel and a matching set of probes in the intervention vehicle. Funnel devices are attached to the top part of the docking structure and distributed to match the three probes mounted on the frame of the Girona 500 I-AUV [15]. In its current state (see Fig. 2), the vehicle must exert forward thrust to stay docked, however, future implementations will include a latching system. A flat panel is placed in the middle of the funnels. Its texture-rich surface allows us to use feature-based algorithms to detect its pose using a digital camera (see Section III). To avoid that water turbidity may limit the range in which the panel is detected, the panel will be equipped with an acoustic transponder for long range detection in a near future [16]. Two more panels are placed on the lower part of the structure. Those contain the mock-ups of a $1/4$ turn valve and a funnel shaped hot stab connector, used to demonstrate the intervention capabilities (see Section VII). Because the arm used for the intervention has a very restricted working area (only 4 DoF), these two panels have been designed to align the axis of the forearm with the valve and the connector.

III. Panel detection & vehicle localization

The subsea panel is detected by a vision-based algorithm that compares the images gathered by the vehicle's front camera against an *a priori* known template of the panel. For each gathered image, a set of features is extracted and matched against the pre-computed set of features detected in the *a priori* known template. When a sufficient number of these features are matched, the position/orientation of the panel can be accurately estimated. The proposed algorithm, uses the oriented FAST and rotated BRIEF(ORB) ([17]) feature extractor for its suitability for real-time applications. The ORB feature extractor detects key-points in the image. Due to the man-made nature of the docking panel, multiple key-points are detected in the object of interest. Compared with feature extractors such as scale invariant feature transform (SIFT) [18] and speeded-up robust features (SURF) [19], BRIEF allows real-time matching of key-points at higher image frame-rates.

Vehicle localization is achieved by merging the data of several navigation sensors (i.e. a Doppler velocity log (DVL), an attitude and heading reference unit (AHRS), a depth sensor, and a global positioning system (GPS)) through an extended Kalman filter (EKF). However, when the vehicle is submerged and GPS data is no longer available, vehicle's position uncertainty starts growing in both x and y axis. To avoid this situation, a single landmark simultaneous localization and mapping (SLAM) algorithm has been implemented using the pose of the detected panel as a landmark. This method improves the pose in which the panel is detected while keeping the I-AUV position covariance bounded. The state vector proposed for this EKF-SLAM algorithm is:

$$\mathbf{x}_k = [x\ y\ z\ u\ v\ w\ l_x\ l_y\ l_z\ l_\phi\ l_\theta\ l_\psi]^T, \tag{1}$$

where $[x\ y\ z\ u\ v\ w]$ are vehicle position (in world coordinates) and linear velocity (with respect the vehicle's frame), and $[l_x, l_y, l_z, l_\phi, l_\theta, l_\psi]$ is the panel pose (in world coordinates).

A constant velocity kinematics model is used to determine how the vehicle state will evolve from time $k-1$ to k. The predicted state at time k, $\mathbf{x}_k^-$ follows the equation:

$$\mathbf{x}_k^- = f(\mathbf{x}_{k-1}, \mathbf{n}_{k-1}, \mathbf{u}_k, t), \tag{2}$$

$$\mathbf{x}_k^- = \begin{bmatrix} \begin{bmatrix} x_{k-1} \\ y_{k-1} \\ z_{k-1} \end{bmatrix} + \mathbf{R}(\phi_k \theta_k \psi_k) \left(\begin{bmatrix} u_{k-1} \\ v_{k-1} \\ w_{k-1} \end{bmatrix} t + \begin{bmatrix} n_{u_{k-1}} \\ n_{v_{k-1}} \\ n_{w_{k-1}} \end{bmatrix} \frac{t^2}{2} \right) \\ \begin{matrix} u_{k-1} + n_{u_{k-1}} t \\ v_{k-1} + n_{v_{k-1}} t \\ w_{k-1} + n_{w_{k-1}} t \\ l_{x_{k-1}} \\ l_{y_{k-1}} \\ l_{z_{k-1}} \\ l_{\phi_{k-1}} \\ l_{\theta_{k-1}} \\ l_{\psi_{k-1}} \end{matrix} \end{bmatrix}$$

where t is the time period, $\mathbf{u} = [\phi\ \theta\ \psi]$ is the control input given by the vehicle AHRS, which determines the current vehicle orientation, and $\mathbf{n} = [n_u\ n_v\ n_w]$ is a vector of zero-mean white Gaussian acceleration noise.

Four measurement updates are applied to the filter: DVL velocities ($[u, v, w]$), depth sensor ($[z]$) and GPS ($[x, y]$) positions, and landmark (i.e. panel pose) updates ($[l_x, l_y, l_z, l_\phi, l_\theta, l_\psi]$). All these updates follow the model:

$$\mathbf{z}_k = \mathbf{H}\mathbf{x}_k + \mathbf{s}_k, \tag{3}$$

where $\mathbf{z}_k$ is the measurement itself, $\mathbf{H}$ is the observation matrix that relates the state vector with the sensor measurement, and $\mathbf{s}_k$ is the sensor noise. While the $\mathbf{H}$ matrices for position and velocity updates are trivial, the observation matrix for the landmark update is:

$$\mathbf{H} = \begin{bmatrix} -\mathbf{Rot}^T & \mathbf{0}_{3\times3} & \mathbf{Rot}^T & \mathbf{0}_{3\times3} \\ \mathbf{0}_{3\times3} & \mathbf{0}_{3\times3} & \mathbf{0}_{3\times3} & \mathbf{I}_{3\times3} \end{bmatrix}, \tag{4}$$

where $\mathbf{I}_{3\times3}$ denotes the 3×3 identity matrix, $\mathbf{0}_{3\times3}$ denotes the 3×3 zero matrix, and $\mathbf{Rot}$ is the vehicle orientation rotation matrix.

IV. Docking

The docking maneuver to be demonstrated is composed by four steps: i) the intervention panel must be detected and mapped by the EKF-SLAM algorithm; ii) the I-AUV has to approach the panel; iii) once closer a dock homing procedure is executed; and iv) the vehicle pushes forward to finalize the mechanical coupling. The Girona 500 I-AUV has several control modes that can be used to move it but all of them make use of its low-level controller. This low-level controller is a cascade control scheme that allows to control the vehicle by means of pose (position + orientation), twist (linear velocity + angular velocity), and wrench (force + torque) requests. In general, the output of the first stage of a cascade control scheme is the input of the second and so on. Therefore, when a high level controller requests a desired pose this is transformed into a desired twist, then into a desired wrench, and finally into a desired setpoint for each thruster. However, in our proposed implementation each DoF is treated independently. Thus the high level controller may request a desired pose, for instance in z or ψ, while also requesting a desired velocity in u or a wrench in any other DoF (see Fig. 3).

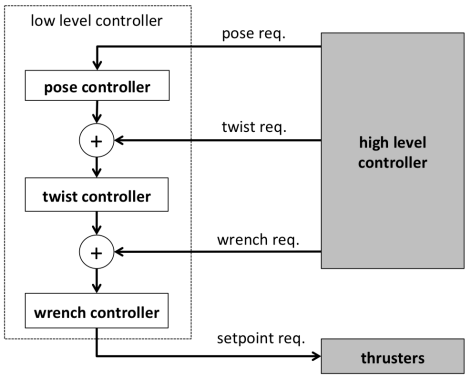

Fig. 3: Girona 500 I-AUV low level cascade control scheme.

To reach the panel a waypoint called *approaching waypoint*, placed at 2m in front of the panel, is generated. The orientation error (ψ_e) between vehicle's current pose and the *approaching waypoint* is computed according to (5) and requested to the pose controller together with the waypoint's depth.

$$\begin{aligned} \Delta_x &= x'(t) - x(t), \\ \Delta_y &= y'(t) - y(t), \\ \psi_e(t) &= atan2(\Delta_y, \Delta_x). \end{aligned} \tag{5}$$

When, $\psi_e(t)$ is smaller than a user-defined error ($angle\_error$), the desired surge (u) is also requested to the velocity controller following:

$$\begin{aligned} u'(t) = \quad & min\left(\frac{\sqrt{\Delta_x^2 + \Delta_y^2}}{approach\_factor}, 1 \right) \cdot \\ & \left(1 - \frac{\mid \psi_e(t) \mid}{angle\_error} \right) \cdot max\_surge, \end{aligned} \tag{6}$$

with $angle\_error = 0.3\ rad$, $approach\_factor = 4$ and $max\_surge = 0.6\ m/s$ for Girona 500 I-AUV. When the vehicle reaches a position which euclidean distance from the *approaching waypoint* is smaller than a user defined error (i.e. 0.5 m in our case), the waypoint is considered achieved. For the homing procedure (step iii) a second waypoint called *docking waypoint*, in which the vehicle probes are nearly inside the docking funnel-shaped receptacles, is computed. While in the previous control mode the vehicle was only requested to move to a desired position ($[x, y, z]$) now it is requested to move to a specific position and orientation ($[x, y, z, \psi]$). Thus, for the homing procedure, the pose controller is in charge to move the vehicle, following the whole cascade control scheme.

If during the homing procedure the panel has been detected by the vision detection algorithm, providing an accurate position for both vehicle and intervention panel, the docking maneuver finalizes requesting the I-AUV to *push* forward (i.e. requesting $X = 35N$ to the wrench controller) while keeping the linear velocity w and the angular velocity ψ at zero (step iv). Otherwise, if the vision system is unable

to detect the panel while performing the homing procedure, this step is aborted and the vehicle returns to the *approaching waypoint*.

V. Valve and Connector Detection

For the valve/connector detection, a stereo camera has been placed in the bottom hull of the Girona 500 I-AUV pointing to the region where the valve/connector is supposed to be once the vehicle is docked. The three valve ends have been painted in order to detect its pose and rotation (allowing 90° turns). Because the connector is not able to rotate, only its pose is estimated. Two detection methods have been implemented, a HSV color detection for the valve and a marker detection for the connector. These algorithms can run individually or simultaneously to increase robustness.

The first method uses the histogram of hue and saturation in the HSV color space [10]. This method has been adapted to detect the three painted marks on the valve in both cameras. The 3D position of the detected blobs are computed by triangulation, and then the positions are matched to their known 3D model using an optimal rigid transformation (see Fig. 4). This transformation is defined as follows:

$$B = R \cdot A + t, \tag{7}$$

where A and B are the points of the detected valve and the known 3D model respectively. R is the rotation from the actual valve points to the 3D model frame and t is the translation between their origins. The 3D model of the valve is defined at the origin of the camera frame. Therefore, computing the optimal rotation and translation between the 3D world points and the model will result in the homogeneous transformation that defines the pose of the valve relative to the camera frame. To solve equation (7) both datasets are moved to the same origin and singular value decomposition (SVD) is applied to find the optimal rotation:

$$H = \sum_{i=1}^{N} (P_A^i - C_A)(P_B^i - C_B), \tag{8}$$

$$[U, S, V] = \text{SVD}(H), \tag{9}$$

$$R = V \cdot U^T, \tag{10}$$

where N is the number of points, P^i represents the ith-point of the corresponding dataset and C_A/C_B are the centroids of A and B. Once the optimal rotation has been found, the translation can be computed as follows:

$$t = -R \cdot C_A + C_B. \tag{11}$$

The transformation between the valve and the connector is static due to the rigid structure that joins them and can be easily measured.

Alternatively, an ARToolkit [20] marker has been placed near to the hot stab connector to provide a more accurate pose of this element. The ARToolkit library provides methods for detecting the marker using a non-stereo camera as well as determining the position and orientation of the marker with respect to it. It is worth noting than the ARMarker is not on the connector but near it, so the static transformation between the ARMarker and the connector must be also measured. If both detectors are running simultaneously, the first one is used to estimate the valve's position/rotation while the latter is used for estimating the connectors position. If only one is running, the pose of the unknown actuator is computed assuming the measured transformation between them.

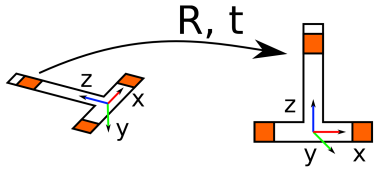

Fig. 4: Valve optimal rigid transformation.

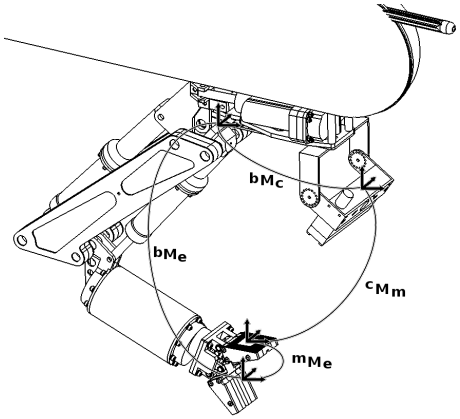

Fig. 5: Manipulation system frames and transformations.

VI. Arm Initialization and Visual Servoing

Prior to the experiment, the arm must be initialized to know its zero position in the joint space because the positions given by the hall sensors are relative. To this aim, each joint is moved to its mechanical limit and its zero position is fixed. Later on, the hall effect sensors, located in the electrical motors, are used to track the joint angles. Nevertheless, the uncertainty in the kinematics model and the non linearities in the linear-to-circular transmission used to move the rotative joints by means of electrical driven pistons are responsible for the inaccuracy of the Cartesian position of the end-effector, in particular at the boundaries of the working space. To solve this issue, a visual servoing approach has been followed. An ARMarker, like the one presented in the previous section, has been placed in the jaw grip to compute the real position of each joint every time that the ARMarker is in the camera's field of view.

In order to obtain the relation between the base of the arm and the camera (${}^bM_c$) (see Fig. 5), the arm is placed in a position where the camera can clearly see the ARMarker. On one hand, the camera-to-marker transformation (${}^cM_m$) is estimated using the ARToolkit library. On the other hand, the transformation from the arm base to the end-effector (${}^bM_e$) is

obtained using the arm forward kinematics. With these two transformations and the fixed relation between the marker and the end-effector ($^{m}M_{e}$), the desired relation ($^{b}M_{c}$) is computed as follows:

$$^{b}M_{c} = ^{b}M_{e} \cdot (^{c}M_{m} \cdot ^{m}M_{e})^{-1}. \quad (12)$$

During the intervention, each time that the ARMarker pose is estimated, the transformation between the arm base and the end-effector is computed applying:

$$^{b}M_{e} = ^{b}M_{c} \cdot ^{c}M_{m} \cdot ^{m}M_{e} \quad (13)$$

The position for each joint can be computed applying inverse kinematics to the obtained transformation $^{b}M_{e}$. Next, the difference between the position estimated by the visual servoing algorithm and the one measured by the internal hall effect sensors is computed.

$$offset_{[1,\cdots,n]} = estimated_{[1,\cdots,n]} - internal_{[1,\cdots,n]}. \quad (14)$$

Between two ARMarker detections, the position of each joint is obtained by adding the measured joint position (hall effect sensors) with their offset. This approach reduces the arm inaccuracies ensuring the pose consistency between the end-effector and the robot base.

VII. Valve Turning and Connector Unplugging/Plugging

The intervention phase starts once the vehicle is docked and the detections are available. Two operations are performed: turn a valve and unplug/plug a hot stab connector. The main steps followed for the intervention are summarized hereinafter. Given an object to manipulate (valve or connector) and given its pose relative to the camera ($^{c}M_{o}$), the pose of the object with respect to the arm-base can be easily computed as follows.

$$^{b}M_{o} = ^{b}M_{c} \cdot ^{c}M_{o} \quad (15)$$

Next, two waypoints are defined for the valve: pre-manipulation and manipulation. And four for the connector: pre-manipulation, manipulation, unplug and plug. To reach each one of these waypoints, the system computes the Cartesian distance from the end-effector to the desired waypoint (x_e). This distance is multiplied by the pseudo-inverse of the arm Jacobian at the end-effector (J_e^+), obtaining the joint velocities ($\dot{q}$) that drive the arm in the Cartesian space to the desired waypoint:

$$\dot{q} = J_e^+ \cdot x_e. \quad (16)$$

Since the arm only has 4 DoF, the orientation in which the waypoints are reached is not taken into account, so the last three rows in the Jacobian, which are referred to the orientation, are set to zero.

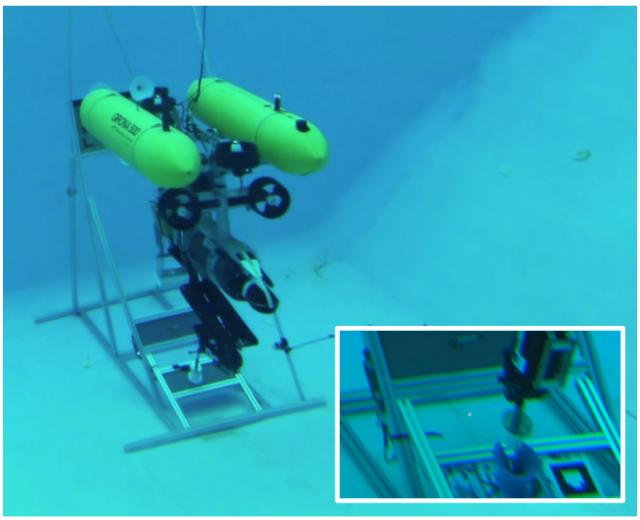

Fig. 6: Girona 500 I-AUV docked in a subsea panel unplugging a hot stab connector.

VIII. Results

This paper presents a combination of several algorithms to perform an autonomous underwater panel intervention. This unmanned intervention consists in docking a vehicle into an adapted intervention panel in order to turn a valve and plug/unplug a hot stab connector. To the best of the authors knowledge, this kind of autonomous intervention has never been demonstrated with a light-weight I-AUV.

To validate all the algorithms involved in this task the following setup has been prepared. A mock-up of an intervention panel has been deployed in a water tank of 16 $\times$ 8 $\times$ 5 meters. The Girona 500 I-AUV [15] was used in these experiments. It has been equipped with a passive docking system, consisting of three probes, and an ECA 4 DoF manipulator [21] (see Fig. 6). Two cameras have also been mounted on the vehicle: one, looking forward to estimate the panel pose and the other pointing down to detect the intervention objects to be manipulated as well as to improve the manipulator's end-effector pose (see sections V and VI).

For testing the docking phase, the I-AUV was teleoperated to a location where the intervention panel was within the the camera field of view, so that, the EKF-SLAM algorithm mapped the panel as a landmark. Next, the vehicle was placed to a random position in the water tank and the autonomous docking maneuver was started. The docking phase was successfully repeated 11 out of 12 times. In 6 of these tests a Seaeye MCT1 thruster was used to generate currents in the water tank. The thruster was placed next to the intervention panel and its setpoint was changed every 20 seconds to a random value between the 30% and 70% of its maximum 14kg thrust. The precision achieved after the homing procedure, where the vehicle probes should be aligned and nearly touching the funnels in the panel (see Section IV), was: $\sigma_x = 2.07\ cm$, $\sigma_y = 3.76\ cm$, $\sigma_z = 1.9\ cm$, and $\sigma_\psi = 0.76°$. These errors were small enough to achieve the mechanical coupling between the vehicle probes

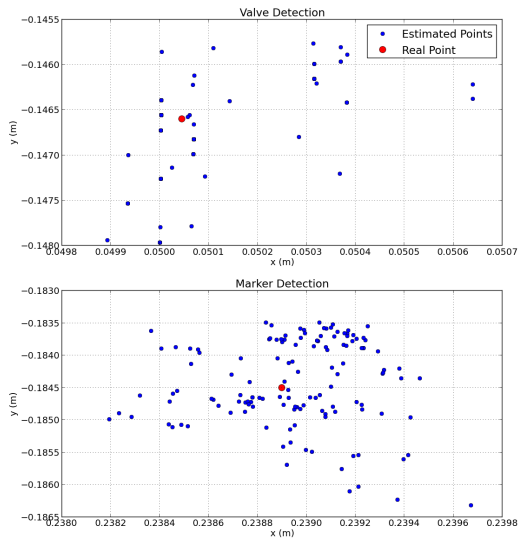

Fig. 7: Valve detection (top) and ARMarker (bottom) estimations in x/y plane.

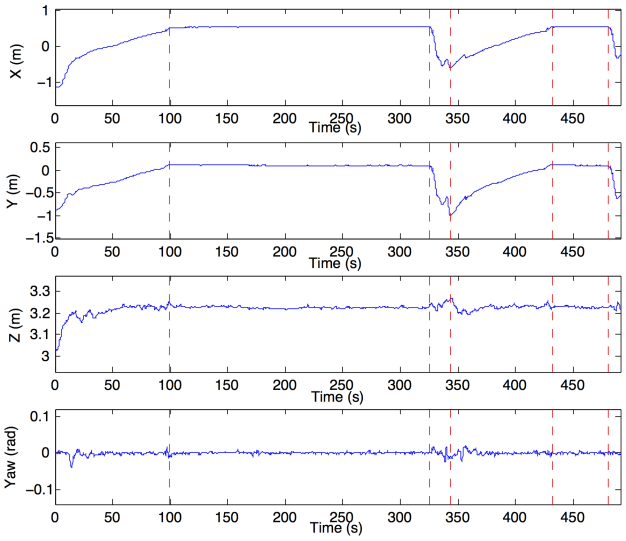

Fig. 8: Vehicle pose during the whole intervention task.

and the funnels in the panel when the I-AUV pushed forward. The average time to complete the docking procedure was 115 seconds.

Both valve and connector detections were influenced by light changes and occlusions. Even so, the system has been designed to work under tenths of meters, where darkness is guaranteed and constant artificial lightning must be used. Regarding the valve detection, the size and shape of the marks changed depending on the vantage point, and the detected centroid was shifted from its actual center, causing small errors. The ARMarker detection showed more reliability when the marker was closer to the camera, so that the total size in pixels was bigger and therefore the computation of its pose was more precise. To estimate the repeatability of these errors, a *static test* was performed assuming the structure of the I-AUV fixed when it was docked and the arm was not moving. Figure 7 illustrates the valve/connector pose estimations during a *static test* of 30 seconds. The lower number of points for the valve detection plot is due to the low frequency rate of this algorithm. The repeatability error for the valve detection was $0.57\ mm$ with a standard deviation of $0.53\ mm$ whilst for the ARMarker the average error was $0.9\ mm$ with a standard deviation of $0.79\ mm$.

Figure 8 shows the I-AUV trajectory while performing the whole intervention task. During the first 99 seconds the I-AUV docked into the intervention panel. Up to second 325, the vehicle was performing a valve turning and the unplugging of the hot stab connector. Next, the vehicle was automatically undocked and then manually moved to a random position in the water tank. At time 343 seconds, a second docking maneuver was conducted. After 90 seconds, the docking finalized and the connector plugging task was executed. When the connector was plugged again the vehicle undocked at second 481.

Figure 9 shows the trajectory of the end-effector with respect to the base of the arm during the whole intervention, as well as the waypoints that the end-effector attempted to reach. The rough edges present in some trajectories (e.g. from valve pre-manipulation to valve manipulation waypoints) are due to visual servoing algorithm updates in the position of the end-effector. All the waypoints were reached with an average precision of 2 mm between the estimated end-effector position and the desired waypoint.

It is worth noting that several errors are involved in the intervention task: the position error of the intervention objects detected by the vision-based algorithms, the position error of the end-effector obtained from the visual-servoing algorithm combined with the hall sensors, the accuracy error of the arm controller, and the calibration errors (i.e. ${}^{b}M_{c}$, ${}^{m}M_{e}$, ...). Although we have seen that all these errors are of the order of 1-3 mm, their combination can produce errors up to 2 cm. To overcome this larger errors, the hot stab is designed with a funnel shape and the end-effector has been V-shaped to mechanically simplify both turning and plugging/unplugging tasks.

IX. CONCLUSIONS AND LESSONS LEARNED

This paper has presented the integration of several systems in the context of a subsea panel docking and an intervention procedure performed by the light-weight I-AUV Girona 500. To simplify the overall task, an AUV-friendly intervention panel has been designed and built. Adapting the panel to our vehicle has been a key element on the overall mission success. The feature-based vision algorithm to estimate the panel pose combined with the navigation data gathered by the I-AUV sensors in an EKF-SLAM algorithm has demonstrated to be a reliable solution to improve both the vehicle and panel position. Regarding the other vision-based algorithms developed to estimate the position of the elements of interest (i.e. the valve to turn and the connector to plug/unplug) as well as to improve the estimation of the end-effector position

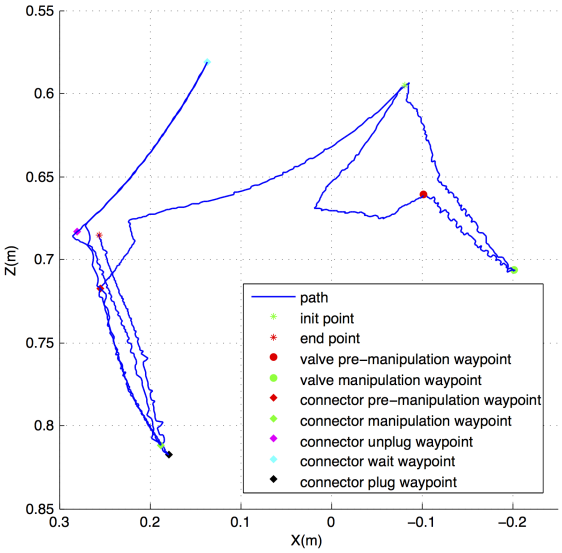

Fig. 9: End-effector Cartesian trajectory during the intervention.

(through a visual servoing algorithm) it must be said that ARMarker-based solutions have been more robust than color-based approaches. While the former have worked out of the box the latter have required adjustments due to light changes. Initial problems with the position of the manipulator's end-effector have bee overcome with the inclusion of a visual servoing algorithm that has substantially improved the arm accuracy. The paper, and the accompanying video, reports two consecutive intervention maneuvers in a water tank. In the first one, the I-AUV docks, turns a valve and unplugs a hot stab connector before undocking. In the second, the I-AUV (still holding the connector) docks again, plugs the connector, and undocks.

To accomplish the final scenario proposed in the TRITON project, this same experiment has to be carried out at sea. To that end, a transponder will be attached to the intervention panel and a range-only localization algorithm [16] will be used to detect the panel and navigate towards it. Once the panel appears in the vehicle's field of view, the docking and intervention tasks detailed in this paper will be repeated.

REFERENCES

[1] H. H. Wang, S. M. Rock, and M. J. Lees, "Experiments in automatic retrieval of underwater objects with an AUV," *OCEANS '95. MTS/IEEE. Challenges of Our Changing Global Environment. Conference Proceedings*, vol. 1, pp. 366–373, 1995.

[2] S. Choi, G. Takashige, and J. Yuh, "Experimental study on an underwater robotic vehicle: ODIN," *AUV'94. Proceedings of the 1994 Symposium Autonomous Underwater Vehicle Technology*, pp. 79–84, 1994.

[3] V. Rigaud, E. Coste-Maniere, M. Aldon, P. Probert, M. Perrier, P. Rives, D. Simon, D. Lang, J. Kiener, A. Casal, J. Amar, P. Dauchez, and M. Chantler, "UNION: underwater intelligent operation and navigation," *Robotics & Automation Magazine, IEEE*, vol. 5, no. 1, pp. 25–35, 1998.

[4] D. Lane, D. J. O'Brien, M. Pickett, J. Davies, G. Robinson, D. Jones, E. Scott, G. Casalino, G. Bartolini, G. Cannata, A. Ferrara, D. angeletti, G. Veruggio, R. Bono, P. Virgili, M. Canals, R. Pallas, E. Garcia, and C. Smith, "AMADEUS-Advanced Manipulation for Deep Underwater Sampling," *IEEE Robotics and Automation Magazine*, vol. 4, no. 4, pp. 34–45, 1997.

[5] J. Evans, K. Keller, J. Smith, P. Marty, and O. Rigaud, "Docking techniques and evaluation trials of the SWIMMER AUV: an autonomous deployment AUV for work-class ROVs," *OCEANS, 2001. MTS/IEEE Conference and Exhibition*, vol. 1, pp. 520–528, 2001.

[6] B. Fletcher, C. Young, J. Buescher, L. Whitcomb, A. Bowen, R. McCabe, and D. Yoerger, "Proof of concept demonstration of the Hybrid Remotely Operated Vehicle (HROV) light fiber tether system," *OCEANS 2008*, pp. 1–6, 2008.

[7] N. Farr, A. Bowen, J. Ware, C. Pontbriand, and M. Tivey, "An integrated, underwater optical /acoustic communications system," in *OCEANS 2010 IEEE - Sydney*, 2010, pp. 1–6.

[8] J. Evans, P. Redmond, C. Plakas, K. Hamilton, and D. Lane, "Autonomous docking for Intervention-AUVs using sonar and video-based real-time 3D pose estimation," *OCEANS 2003*, vol. 4, pp. 2201–2210, 2003.

[9] G. Marani, S. Choi, and J. Yuh, "Underwater Autonomous Manipulation for Intervention Missions AUVs," *Ocean Engineering. Special Issue: AUV*, vol. 36, no. 1, pp. 15–23, 2009.

[10] M. Prats, D. Ribas, N. Palomeras, J. Garcia, V. Nannen, S. Wirth, J. J. Fernandez, J. Beltran, R. Campos, P. Ridao, P. Sanz, G. Oliver, M. Carreras, N. Gracias, R. Marin, and A. Ortiz, "Reconfigurable auv for intervention missions: a case study on underwater object recovery," *Intelligent Service Robotics*, vol. 5, no. 1, pp. 19–31, 2012. [Online]. Available: http://dx.doi.org/10.1007/s11370-011-0101-z

[11] M. Prats, J. García, S. Wirth, D. Ribas, P. Sanz, P. Ridao, N. Gracias, and G. Oliver, "Multipurpose autonomous underwater intervention: A systems integration perspective," *Control & Automation (MED), 2012 20th Mediterranean Conference on*, pp. 1379–1384, 2012.

[12] P. J. Sanz, P. Ridao, G. Oliver, G. Casalino, Y. Petillot, C. Silvestre, C. Melchiorri, and A. Turetta, "TRIDENT: An european project targeted to increase the autonomy levels for underwater intervention missions," in *OCEANS'13 MTS/IEEE*, 2013.

[13] S. Krupinski, F. Maurelli, A. Mallios, and P. Sotiropoulos, "Towards AUV docking on sub-sea structures," in *OCEANS 2009 MTS/IEEE*, 2009.

[14] P. Sotiropoulos, D. Grosset, G. Giannopoulos, and F. Casadei, "AUV docking system for existing underwater control panel," in *OCEANS 2009 MTS/IEEE*, 2009.

[15] D. Ribas, N. Palomeras, P. Ridao, M. Carreras, and A. Mallios, "Girona 500 AUV, from survey to intervention," *IEEE/ASME Transactions on Mechatronics*, vol. 17(1), pp. 46–53, February 2012.

[16] G. Vallicrosa, P. Ridao, and D. Ribas, "Active range-only beacon localization for AUV homing," in *PENDING TO BE ACCEPTED ON Intelligent Robots and Systems (IROS), 2014 IEEE/RSJ International Conference on*, 2014, pp. –.

[17] E. Rublee, V. Rabaud, K. Konolige, and G. Bradski, "ORB: An efficient alternative to SIFT or SURF," in *Computer Vision (ICCV), 2011 IEEE International Conference on*, nov. 2011, p. 25642571.

[18] D. G. Lowe, "Distinctive Image Features from Scale-Invariant Keypoints," *Int. J. Comput. Vision*, vol. 60, no. 2, p. 91110, Nov. 2004.

[19] H. Bay, A. Ess, T. Tuytelaars, and L. Van Gool, "Speeded-Up Robust Features (SURF)," *Comput. Vis. Image Underst.*, vol. 110, no. 3, p. 346359, Jun. 2008.

[20] H. Kato and M. Billinghurst, "Marker tracking and hmd calibration for a video-based augmented reality conferencing system," in *Augmented Reality, 1999. (IWAR '99) Proceedings. 2nd IEEE and ACM International Workshop on*, 1999, pp. 85–94.

[21] J. Fernandez, M. Prats, P. Sanz, J. Garcia, R. Marin, D. Robinson, M. Ribas, and P. Ridao, "Grasping for the seabed: Developing a new underwater robot arm for shallow-water intervention," *Robotics Automation Magazine, IEEE*, vol. 20, no. 4, pp. 121–130, Dec 2013.